

A Phase Transition in Diffusion Models Reveals the Hierarchical Nature of Data

Antonio Sclocchi¹ Alessandro Favero¹ Matthieu Wyart¹

Abstract

Understanding the structure of real data is paramount in advancing modern deep-learning methodologies. Natural data such as images are believed to be composed of features organised in a hierarchical and combinatorial manner, which neural networks capture during learning. Recent advancements show that diffusion models can generate high-quality images, hinting at their ability to capture this underlying structure. We study this phenomenon in a hierarchical generative model of data. We find that the backward diffusion process acting after a time t is governed by a phase transition at some threshold time, where the probability of reconstructing high-level features, like the class of an image, suddenly drops. Instead, the reconstruction of low-level features, such as specific details of an image, evolves smoothly across the whole diffusion process. This result implies that at times beyond the transition, the class has changed but the generated sample may still be composed of low-level elements of the initial image. We validate these theoretical insights through numerical experiments on class-unconditional ImageNet diffusion models. Our analysis characterises the relationship between time and scale in diffusion models and puts forward generative models as powerful tools to model combinatorial data properties.

1. Introduction

Understanding which data are learnable by algorithms is key to machine learning. Techniques such as supervised, unsupervised, or self-supervised learning are most often used with high-dimensional data. However, in large dimensions, for generic data or tasks, learning should require a number of training examples that is exponential in the dimension (Luxburg & Bousquet, 2004; Bach, 2017), which is never achievable in practice. The success of these meth-

¹Institute of Physics, École polytechnique fédérale de Lausanne (EPFL). Correspondence to: <firstname.lastname@epfl.ch>.

Preprint.

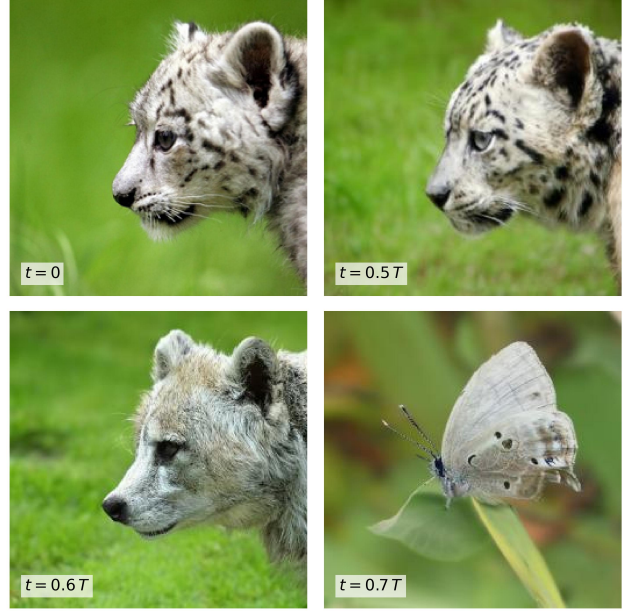


Figure 1. Images generated by a denoising diffusion probabilistic model starting from the top-left image and inverting the dynamics at different times t . T corresponds to the time scale when the forward diffusion process converges to an isotropic Gaussian distribution. At small t , the class of the generated image remains unchanged, with only alterations of low-level features, such as the eyes of the leopard. After a characteristic time t , the class undergoes a phase transition and changes. However, some low-level attributes of the original image are retained to compose the new image. For instance, the wolf is composed with eyes, nose and ears similar to those of the leopard, and the butterfly inherits its colours and black spots.

ods with limited training set sizes, including for images or texts, implies that such data are highly structured. In particular, the puzzling phenomenon central to this work is the ability of generative models to compose a whole new datum by assembling features learned from examples. This feat is remarkable in foundational models generating text, or in diffusion models generating images (Sohl-Dickstein et al., 2015; Ho et al., 2020; Song & Ermon, 2019; Song et al., 2020) – such as DALL·E (Betker et al., 2023) and StableDiffusion (Rombach et al., 2022) – investigated here.

Many theoretical studies in machine learning assume that the data distribution is Gaussian, which is ill-suited to study compositionality. Conversely, we consider hierarchical generative models of data, inspired by models of formal grammar and statistical physics, for which the ability of diffusion-based models to compose can be described exactly.

Diffusion models add noise to images as time increases and learn the reverse denoising process to generate new samples. If some finite amount of noise is added, and the process is then reversed, we predict that (i) for small noise, only low-level features of the image change, as already noticed empirically (Ho et al., 2020), (ii) there exists a threshold noise at which the probability of remaining in the same class suddenly drops to near-random chance and (iii) surprisingly, beyond that point, low-level features may persist and compose the element of a new class. Remarkably, these results appear already evident in examples such as Figure 1 and can be systematically quantified by considering the change of internal representations in state-of-the-art CNNs, whereby a remarkable correspondence to our predictions is found.

Overall, our analysis reveals that diffusion models act at different hierarchical levels of the data at different time scales within the diffusion process. It also puts forward hierarchical generative models as a valuable theoretical tool to address several unanswered questions in machine learning.

1.1. Our contributions

On the theoretical side, we consider models belonging to the class of L -level context-free grammars where the structure of the latent variables is tree-like. We show that the denoising dynamics of diffusion models can be solved exactly for these models of data using belief propagation (BP). In particular, the analytical treatment of BP describes the evolution of the probability of latent variables for different levels of corruption noise and reveals a phase transition for a threshold noise value when L is large. We show numerically that the dynamics of latent variables is reflected in the hidden representation of deep networks previously trained on a supervised classification task on these data.

On the empirical side, we test these insights by performing a systematic study of the denoising diffusion dynamics on ImageNet. Following (Ho et al., 2020), we invert the noising process at some time t , leading to novel noiseless images. We then analyse how the representation of a state-of-the-art convolutional architecture changes between the initial and newly generated images as a function of both time t and depth of the representation. Our results confirm the presence of a sharp transition in the class at a given time or noise level.

1.2. Related work

Theory of diffusion models Most of the theoretical work on diffusion models considers simple models of data. Un-

der mild assumptions on the data distribution, diffusion models exhibit a sample complexity that scales exponentially with the data dimension (Block et al., 2020; Oko et al., 2023). This curse of dimensionality can be mitigated through stronger distributional assumptions, such as considering data lying within a low-dimensional latent subspace (De Bortoli, 2022; Chen et al., 2023; Yuan et al., 2023), Gaussian mixture models (Biroli & Mézard, 2023; Shah et al., 2023; Cui et al., 2023), graphical models (Mei & Wu, 2023), or data distributions that can be factorised across scales (Kadkhodaie et al., 2023). Closer to our work, Okawa et al. (2023) consider synthetic compositional data to empirically show how diffusion models learn to generalise by composing different concepts. In contrast, we study data that are not only compositional but also hierarchically structured and make quantitative predictions on how diffusion models compose features at different scales.

Hierarchical models of data structure Generative models of data have a long history in linguistics (Rozenberg & Salomaa, 1997) and have more recently received attention in the context of machine learning theory. In supervised learning, deep networks can represent hierarchical tasks more efficiently than shallow networks (Poggio et al., 2017) and can efficiently learn them from an information theory viewpoint (Schmidt-Hieber, 2020). For hierarchical models of data, correlations between the input data and the task are critical for learning (Mossel, 2016; Shalev-Shwartz et al., 2017; Malach & Shalev-Shwartz, 2018; 2020) and the representations learnt by neural networks with gradient descent reflect the hidden latent variables of such models both in CNNs (Cagnetta et al., 2023) and transformers (Allen-Zhu & Li, 2020). In this work, we use these hierarchical generative models of data to study the denoising dynamics of diffusion models theoretically.

2. Diffusion models and feature hierarchies

This section introduces denoising diffusion probabilistic models and demonstrates how class-unconditional ImageNet diffusion models operate on image features across different hierarchical levels at different time scales.

2.1. Background on denoising diffusion models

Denoising diffusion probabilistic models (DDPMs) (Ho et al., 2020) are generative models designed to sample from a distribution by reversing a step-by-step noise addition process. In particular, let $q(\cdot)$ represent the data distribution, and let x_0 be a sample drawn from this distribution, i.e., $x_0 \sim q(x_0)$. First, DDPMs consist of a *forward process* which is a Markov chain generating a sequence of noised data $\{x_t\}_{1 \leq t \leq T}$ by introducing isotropic Gaussian noise at each time step t with a variance schedule $\{\beta_t\}_{1 \leq t \leq T}$ as

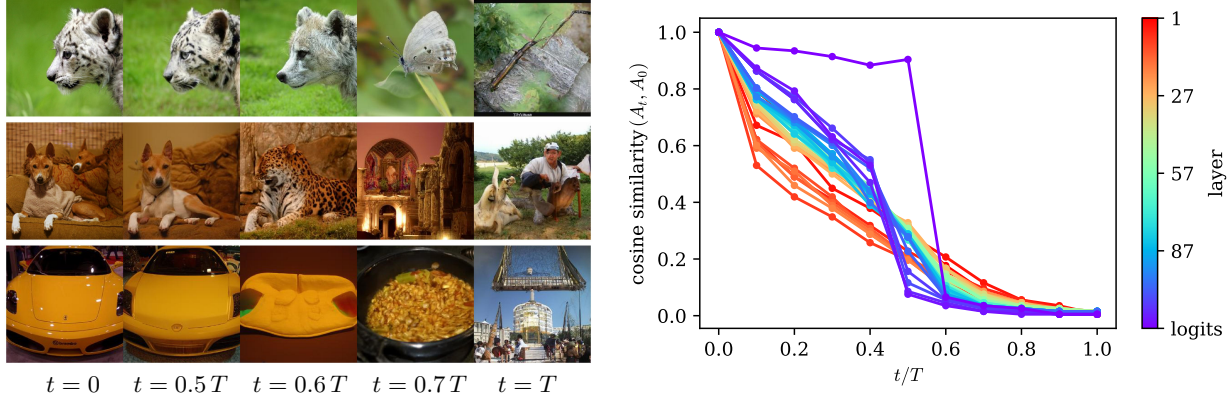


Figure 2. *Left panel.* Examples of images generated by reverting the diffusion process at different times t . Starting from the left images x_0 at time $t = 0$, we generate samples $\hat{x}_0(t) \sim p_\theta(\hat{x}_0|x_t)$ by first running the diffusion process up to time t and then reverting it, as described in Section 2.2. At time $t = T$, x_T corresponds to isotropic Gaussian noise and the generated image $\hat{x}_0(T)$ is uncorrelated from x_0 . At intermediate times, instead, a sudden change of the image class is observed, while some lower-level features are retained. *Right panel.* Cosine similarity between the post-activations of the hidden layers of a ConvNeXt Base (Liu et al., 2022) for the initial images x_0 and the synthesised ones $\hat{x}_0(t)$. Around $t \approx T/2$, the similarity between logits exhibits a sharp drop, indicating the change in class, while the hidden representations of the first layers change more smoothly. This indicates that certain low-level features from the original images are retained for composing the sampled images also after the class transition. To compute the cosine similarity, all activations are standardised, i.e., centred around the mean and scaled by the standard deviation computed on the 50000 images of the ImageNet-1k validation set. At each time, the values of the cosine similarity correspond to the maximum of their empirical distribution over 10000 images (10 per class of ImageNet-1k).

follows:

$$q(x_1, \dots, x_T|x_0) = \prod_{t=1}^T q(x_t|x_{t-1}) \\ = \prod_{t=1}^T \mathcal{N}(x_t; \sqrt{1 - \beta_t}x_{t-1}, \beta_t\mathbb{I}). \quad (1)$$

Thus, at each time step t , we have

$$x_t = \sqrt{\bar{\alpha}_t}x_0 + \sqrt{1 - \bar{\alpha}_t}\eta \quad (2)$$

with $\bar{\alpha}_t = \prod_{t'=1}^t (1 - \beta_{t'})$ and $\eta \sim \mathcal{N}(0, \mathbb{I})$. By selecting the noise schedule such that $\bar{\alpha}_t \rightarrow 0$ as $t \rightarrow T$, the distribution of x_T becomes an isotropic Gaussian distribution. Subsequently, DDPMs reverse this process by gradually removing noise in a *backward process*. In this process, the models learn Gaussian transition kernels $q(x_{t-1}|x_t)$ by parametrising their mean and variance using a neural network with parameters θ as follows:

$$p_\theta(x_{t-1}|x_t) = \mathcal{N}(x_{t-1}; \mu_\theta(x_t, t), \Sigma_\theta(x_t, t)). \quad (3)$$

After training, the learnt p_θ can be used to generate novel examples by initiating the process with $x_T \sim \mathcal{N}(0, \mathbb{I})$ and running it in reverse to obtain a sample from q . We refer the reader to Ho et al. (2020); Nichol & Dhariwal (2021); Dhariwal & Nichol (2021) for more details regarding the formulation of DDPMs and the technical aspects of the reverse transition kernels parameterisation with neural networks.

2.2. Forward-backward experiments

Previous studies on DDPMs noted that inverting the diffusion process at different times t starting from an image x_0 results in samples $\hat{x}_0(t) \sim p_\theta(\hat{x}_0|x_t)$ with distinct characteristics depending on the choice of t . Specifically, when conditioning on the noisy samples x_t 's obtained by diffusing images from the CelebA dataset, one finds that for small values of t , only fine details change (Ho et al., 2020). We conduct a similar experiment using a class-unconditional DDPM introduced by Dhariwal & Nichol (2021) on the ImageNet dataset with 256x256 resolution.

In the left panel of Figure 2, we present some images resulting from this experiment. For each row, the initial image x_0 is followed by images generated by initiating the diffusion process from x_0 , running the forward dynamics until time t , with $0 < t \leq T = 1000$, and ultimately running the backward dynamics to produce a sample image $\hat{x}_0(t)$. Our observations from these synthetic images are as follows:

- (i) Similarly to the findings in Ho et al. (2020), at small inversion times t , only local features change. Furthermore, the class of the sampled images remains consistent with that of the corresponding starting images, i.e., $\text{class}(\hat{x}_0(t)) = \text{class}(x_0)$ with high probability.
- (ii) There exists a characteristic time scale t^* at which the class of the sampled images undergoes a sudden transition.

(iii) Even after the class transitions, some low-level features composing the images persist and are reincorporated into the newly generated image. For instance, looking at the left panel of Figure 2, in the second row, the jaguar is composed with the paws and the ears of the dog in the starting picture, or in the third row, the sofa’s armrests inherit the shape of the car headlights.

Our theory, presented in Section 4 and 5, predicts how features at different hierarchical levels vary at different time scales of the diffusion dynamics in accordance with observations (i), (ii), and (iii).

2.3. ImageNet hidden representations

To quantify the qualitative observations mentioned earlier, we design an experiment using the empirically known fact that deep learning models learn hierarchical representations of the data, with complexity increasing as the architecture’s depth grows. This phenomenon holds true in both real (Olah et al., 2020; LeCun et al., 2015; Zeiler & Fergus, 2014) and synthetic scenarios (Cagnetta et al., 2023; Allen-Zhu & Li, 2020). Therefore, we use these internal representations as a proxy for the compositional structure of the data. We investigate how the hidden representations of a deep ConvNeXt Base model (Liu et al., 2022), achieving 96.9% top-5 accuracy on ImageNet, change as a function of the inversion time t and depth ℓ of the representation. In the right panel of Figure 2, we illustrate the value of the cosine similarity between the post-activations of every hidden layer of the ConvNeXt for the initial and generated images. We observe that:

- (i) The representations of early layers of the network, corresponding to low-level and localised features of the images, are the first to change at short diffusion times and evolve smoothly.
- (ii) At a specific time and noise scale, the similarity between logits experiences a sharp drop, indicating a transition in the class.
- (iii) Around the class transition, there is an inversion of the similarity curves. Indeed, the hidden representations in the first layers for the new and generated images now display the largest alignment. This indicates that low-level features from the original images can be reused in composing the sampled images, as qualitatively observed in Figure 2.

To study the robustness of our results with respect to the architecture choice, in Appendix D, we report the same measurements using ResNet architectures with varying width and depth (He et al., 2016). We find the same qualitative behaviour as the ConvNeXt in Figure 2.

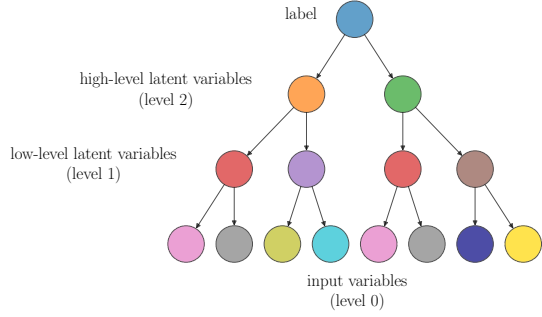


Figure 3. Sketch of the generative hierarchical model we study in the paper. In this example, depth $L = 3$ and branching factor $s = 2$. Different values of the input and latent variables are represented with different colours.

We now present our theory, which predicts these observations. In Section 3, we introduce a generative model of data which mimics the hierarchical and compositional structure of images while being analytically tractable. In Section 4, we solve exactly the denoising process for this model with different levels of noising. Finally, in Section 5, we prove the existence of a phase transition at a critical noise value.

3. Hierarchical generative model of data

To model the combinatorial and hierarchical nature of images, we consider hierarchical generative models (Mosel, 2016; Shalev-Shwartz et al., 2017; Malach & Shalev-Shwartz, 2018; 2020; DeGiuli, 2019; Allen-Zhu & Li, 2020; Cagnetta et al., 2023). Specifically, we study an L -level context-free grammar. It consists of a set of class labels $\mathcal{C} \equiv \{1, \dots, v\}$ and an alphabet $\mathcal{A} \equiv \{a_1, \dots, a_v\}$ of v features. Once the class label γ is picked uniformly at random from \mathcal{C} , the data is generated iteratively from a set of production rules with branching factor s at each level ℓ (see Figure 3, for an illustration):

$$\begin{aligned} \gamma &\mapsto \mu_1^{(L-1)}, \dots, \mu_s^{(L-1)} \text{ for } \gamma \in \mathcal{C} \text{ and } \mu_i^{(L-1)} \in \mathcal{A}, \\ \mu^{(\ell)} &\mapsto \mu_1^{(\ell-1)}, \dots, \mu_s^{(\ell-1)} \text{ for } \mu^{(\ell)} \in \mathcal{A}, \mu_i^{(\ell-1)} \in \mathcal{A}, \\ &\ell \in \{L-1, \dots, 1\}. \end{aligned}$$

Since the total size of the data increases by a factor s at each level, the input data are made of $d \equiv s^L$ input features $\mu^{(0)}$. We adopt a one-hot encoding of these features, ultimately leading to a data vector $X \in \mathbb{R}^{dv}$. Note that for $\ell \geq 1$, the node variables correspond to latent variables, and there is no need to specify any choice of encoding.

For each level ℓ , we consider that there are m distinct production rules originating from the same higher-level feature $\mu^{(\ell)}$, i.e., there are m equivalent lower-level representations

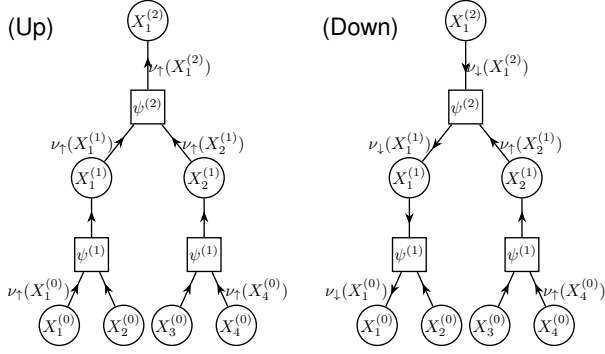


Figure 4. Illustration of the flow of messages in the Belief Propagation algorithm for the case $s = 2$, $L = 2$ of the Random Hierarchy Model. The factor nodes (squares) represent the rules that connect the variables at different levels of the hierarchy. The downward process is represented only for the leftmost branch.

of $\mu^{(\ell)}$. In addition, we assume that two distinct classes or latent variables cannot lead to the same low-level representation. This condition ensures, for example, that two distinct classes never lead to the same data.

We consider the case of the Random Hierarchy Model (RHM) (Cagnetta et al., 2023), for which the m production rules of any latent variable or class are sampled uniformly at random among the v^s possible ones without replacement. In this case, the total number of possible data produced per class is $m \cdot m^s \cdots m^{s^{L-1}} = m^{\frac{d-1}{s-1}}$, where the dimension d is defined as $d = s^L$. In the following, we use the notation $X_i^{(\ell)}$ to indicate the variable at layer ℓ and position $i \in \{1, \dots, s^{L-\ell}\}$.

In the context of unsupervised learning, a key parameter for this model is $f = m/v^{s-1}$. When $f = 1$, all strings of latent variables of size s can be produced at any level of the hierarchy. This implies that all possible v^d input strings are generated, and the data distribution has little structure. When $f < 1$, however, only a small fraction $\sim f^{(d-1)/(s-1)}$ of all possible strings is generated by the production rules. This implies that spatial correlations between different input positions appear, reflecting the hierarchy generating the data.

4. Exact denoising of the RHM with message passing

In this section, we consider the denoising diffusion process for the RHM. Given a noisy observation $X^{(0)} = x(t)$ of the input variables at time t , we compute $p(x(0)|x(t))$ exactly, obtaining full control of the statistics of the diffusion process from time t to time 0. In particular, given the tree structure of the model, we can compute the marginal probability of the values of all latent variables conditioned on $x(t)$

by using a message-passing algorithm. Therefore, we obtain the probability that a latent variable at level ℓ has changed when performing the forward-backward diffusion process for a duration t , a central quantity to interpret Figure 2.

For computing the marginal distributions, we use Belief Propagation (BP) (Mossel, 2001; Mezard & Montanari, 2009), which gives exact results for a tree graph such as the Random Hierarchy Model. In this case, the leaves of the tree correspond to the input variables at the bottom layer, and the root corresponds to the class variable at the top of the hierarchy. Each rule connecting variables at different levels corresponds to a factor node, as shown in Figure 4.

The forward process adds noise to the variables in the input nodes. Each of these nodes sends its *belief* on its value at $t = 0$ to its parent latent node. These beliefs, or *messages*, represent probabilistic estimates of the state of the sender node. Each latent node receives messages from all its children, updates its belief about its state, and sends its *upward message* to its parent node. This process is repeated iteratively until the root of the tree. Subsequently, starting from the root, each node sends a *downward message* to its children. Finally, the product of the upward and downward beliefs received at a given node represents the marginal probabilities of its state conditioned on the noisy observation. Hence, we can use these conditional marginals to compute the mean values of the variables at all levels of the hierarchy. We assume that the production rules of the model are known by the inference algorithm, which corresponds to the optimal denoising process.

The input variables $X^{(0)}$, in their one-hot-encoding representation, undergo the forward diffusion process of Equation 2, which can be defined in continuous time and constant β_t by redefining $\bar{\alpha}_t = e^{-2t}$ and taking the limit $T \rightarrow \infty$ (Song et al., 2020).

The denoising is made in two steps: the initialisation of the messages at the leaves and the BP iteration.

Initialisation of the upward messages In its one-hot-encoding representation, $X_i^{(0)}$ is a v -dimensional vector: taking the symbol $a_\gamma \in \{a_1, \dots, a_v\} = \mathcal{A}$ corresponds to $X_i^{(0)} = e_\gamma$, with e_γ a canonical basis vector. Its continuous diffusion process takes place in \mathbb{R}^v : given the value $X_i^{(0)} = x_i(t)$, we can compute the probability of its starting value $p(x_i(0)|x_i(t))$ using Bayes formula. As derived in Appendix A, we obtain

$$p(x_i(0) = e_\gamma | x_i(t)) = \frac{1}{Z} e^{x_{i,\gamma}(t)/\Delta_t}, \quad (4)$$

with $\Delta_t = (1 - \bar{\alpha}_t)/\sqrt{\bar{\alpha}_t}$ and $Z = \sum_{\mu=1}^v e^{x_{i,\mu}(t)/\Delta_t}$. This computation is performed independently for each input variable i , and therefore does not take into account the spatial

correlations given by the generative model. The probabilities of Equation 4 are used to initialise the BP upward messages $\nu_{\uparrow}^{(0)} = p(x_i(0)|x_i(t))$ at the input variables.

BP iteration Let $\psi^{(\ell)}$ be any factor node connecting an s -tuple of low-level variables at layer $\ell - 1$, $\{X_i^{(\ell-1)}\}_{i \in [s]}$, to a high-level variable $X_1^{(\ell)}$ at layer ℓ . Without loss of generality, to lighten the notation, we rename the variables as $Y = X_1^{(\ell)}$, taking values $y \in \mathcal{A}$, and $X_i = X_i^{(\ell-1)}$, each taking values $x_i \in \mathcal{A}$. For each possible association $y \rightarrow x_1, \dots, x_s$, the factor node $\psi^{(\ell)}(y, x_1, \dots, x_s)$ takes values

$$\psi^{(\ell)}(y, x_1, \dots, x_s) = \begin{cases} 1, & \text{if } y \rightarrow (x_1, \dots, x_s) \text{ is rule at layer } \ell \\ 0, & \text{otherwise.} \end{cases}$$

The BP upward and downward iterations for the (unnormalised) upward and downward messages respectively read

$$\begin{aligned} \tilde{\nu}_{\uparrow}^{(\ell+1)}(y) &= \sum_{x_1, \dots, x_s \in \mathcal{A}^{\otimes s}} \psi^{(\ell+1)}(y, x_1, \dots, x_s) \prod_{i=1}^s \nu_{\uparrow}^{(\ell)}(x_i), \\ \tilde{\nu}_{\downarrow}^{(\ell)}(x_1) &= \sum_{\substack{x_2, \dots, x_s \in \mathcal{A}^{\otimes (s-1)} \\ y \in \mathcal{A}}} \psi^{(\ell+1)}(y, x_1, \dots, x_s) \\ &\quad \times \nu_{\downarrow}^{(\ell+1)}(y) \prod_{i=2}^s \nu_{\uparrow}^{(\ell)}(x_i), \end{aligned} \quad (5)$$

where $\nu_{\rho}^{(\ell)}(x) = \frac{\tilde{\nu}_{\rho}^{(\ell)}(x)}{\sum_{x'} \tilde{\nu}_{\rho}^{(\ell)}(x')}$, $\rho \in \{\uparrow, \downarrow\}$. The downward iteration, reported for x_1 , can be trivially extended to the other variables x_i by permuting the position indices. The values of $\nu_{\uparrow}^{(0)}(x_i)$ and $\nu_{\downarrow}^{(L)}(y)$ are set by the initial conditions. In particular, we initialise $\nu_{\uparrow}^{(0)}(x_i)$ as described in the previous paragraph and $\nu_{\downarrow}^{(L)}(y) = 1/v$, which corresponds to a uniform prior over the possible classes \mathcal{C} .¹

Exact solution We solve the BP upward and backward iterations numerically. In Figure 5, we show the probability corresponding to the correct symbol for each node of the tree. Remarkably, we note that (i) the probability for the correct class at layer L displays a transition at a characteristic time which becomes sharper for increasing L , and (ii) the messages for the correct input variables and the correct latent variables at low levels of the tree change smoothly. In particular, the curves for messages at layer L and layers $\ell < L$ invert their order at the transition, as in our observations on DDPMs and ImageNet data in Figure 2. This transition is our key finding, which we explain below.

¹This assumption corresponds to unconditioned diffusion, where the DDPM is not biased towards any specific class.

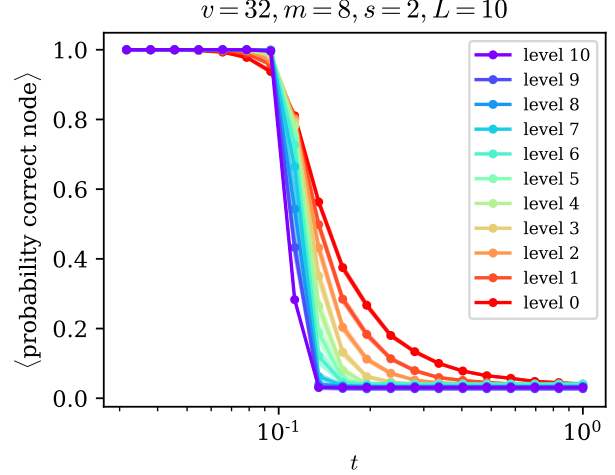


Figure 5. Probability that the latent has not changed in the denoising process, corresponding to the largest marginal probability computed by BP, averaged for each layer, for varying inversion times of the diffusion process t . Data for the RHM with $v = 32$, $m = 8$, $s = 2$, $L = 10$. Each level of the tree, indicated in the legend, is represented with a different colour. We observe the same behaviour of the curves for ImageNet data in Figure 2: the probability of the correct class has a sharp transition at characteristic time scale, while the probabilities corresponding to latent variables in the lower levels change smoothly.

5. Mean-field theory of denoising diffusion

In this section, we make a simplifying assumption for the initial noise acting on the input and adopt a mean-field approximation to justify the existence of a phase transition. Remarkably, this approximation turns out to be of excellent quality for describing the diffusion dynamics. Specifically, consider a reference configuration at the leaves variables $X_i^{(0)} = \bar{x}_i$ that we would like to reconstruct, given a noisy observation of it. We assume that for each leaf variable, the noise is uniformly spread among the other symbols.² In other words, our belief in the correct sequence is corrupted by $\epsilon \in [0, 1]$:

$$\begin{cases} X_i^{(0)} = \bar{x}_i & \text{with belief } 1 - \epsilon, \\ X_i^{(0)} \text{ uniform over alphabet} & \text{with belief } \epsilon. \end{cases} \quad (6)$$

Hence, the initialisation condition of the upward BP messages at a leaf node $X_i^{(0)}$ becomes

$$\begin{cases} \nu_{\uparrow}^{(0)}(\bar{x}_i) &= 1 - \epsilon + \epsilon/v, \\ \nu_{\uparrow}^{(0)}(x_i \neq \bar{x}_i) &= \epsilon/v, \end{cases} \quad (7)$$

where v is the alphabet cardinality.

²This is a mild approximation, as documented in Appendix C

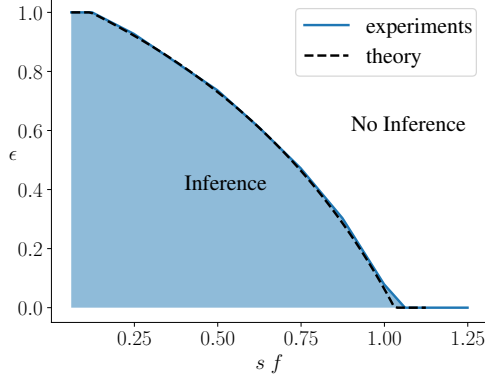


Figure 6. Phase diagram for inferring the class node using the upward iteration of BP. When $sf < 1$, BP can infer the class if $\epsilon < \epsilon^*(sf)$. This transition is very well predicted by our theory. The inference region in the figure corresponds to the phase wherein the probability of the correct class is larger than the initialisation belief in the correct values of the leaves, that is $1 - \epsilon + \frac{\epsilon}{v}$. Experimental data are for a single realisation of the RHM with $v = 32$, $s = 2$, $L = 10$.

Given these initial conditions and since the production rules are known, if $\epsilon = 0$ – i.e., in the noiseless case – BP can reconstruct all the values of the latent variables exactly. Conversely, if $\epsilon = 1$ – i.e., when the input is completely corrupted and the belief on the leaves variables is uniform – the reconstruction is impossible. In general, for a value of ϵ , one is interested in computing the probability of recovering the latent structure of the tree at each layer ℓ and, as $L \rightarrow \infty$, to decide whether the probability of recovering the correct class of the input remains larger than $1/v$.

Upward process We begin by studying the upward process from the leaves. Consider a true input tuple $\bar{x}_1, \dots, \bar{x}_s$ which is associated with the higher-level feature \bar{y} . Given the randomness of the production rules, the messages are random variables depending on the specific realisation of the rules. We adopt a *mean-field* or *annealed* approximation that neglects the fluctuations coming from the random choice of rules. Specifically, we approximate the upward message by the average upward message exiting the corresponding factor node $\langle \nu_{\uparrow}^{(1)}(y) \rangle_{\psi}$ over the possible realisations of ψ .

In Appendix B, we show that $\langle \nu_{\uparrow}^{(1)}(y) \rangle_{\psi}$ can take only two values: one for $y = \bar{y}$ and one for $y \neq \bar{y}$, as expected by symmetry considerations. Therefore, mean messages have the same structure as Equation 7 and we can define a new ϵ' . Introducing the probability of reconstructions $p = 1 - \epsilon + \epsilon/v$ and $p' = 1 - \epsilon' + \epsilon'/v$, we have

$$p' = \frac{p^s + f \frac{m-1}{mv-1} (1 - p^s)}{p^s + f (1 - p^s)} = F(p). \quad (8)$$

Iterating this procedure across all the levels of the tree, we can compute the probability of recovering the correct class of the input. In particular, for large L , we are interested in studying the fixed points $p^* = F(p^*)$ of the iteration map in Equation 8. As derived in Appendix B.1.1, when $sf > 1$, this map has a repulsive fixed point $p^* = 1$, which corresponds to $\epsilon = 0$, and an attractive fixed point $p^* = 1/v$, corresponding to $\epsilon = 1$. Thus, in this regime, inferring the class from the noisy observation of the input is impossible. In contrast, when $sf < 1$, $p^* = 1$ and $p^* = 1/v$ are both attractive fixed points, and a new repulsive fixed point $1/v < p^* < 1$ separating the other two emerges. Therefore, in this second regime, there is a phase transition between a phase in which the class can be recovered and a phase in which it cannot. These theoretical predictions are numerically confirmed in the phase diagram in Figure 6.

Physically, $sf < 1$ corresponds to a regime in which errors at lower levels of the tree do not propagate: they can be corrected using information coming from neighbouring nodes, thanks to the fact that only a small fraction of the strings is consistent with the production rules of the generative model. Conversely, when $sf > 1$, even small corruptions propagate through the entire tree up to the root node and BP cannot infer the class correctly.

Downward process The same calculation can be repeated for the downward process, with the additional difficulty that the downward iteration mixes upward and downward messages. We refer the reader to Appendix B for the theoretical treatment.

Probabilities of reconstruction Combining the mean upward and downward messages, we obtain a theoretical prediction for the probabilities of reconstructing the correct values of the variables at each layer. We compare our theoretical predictions with numerical experiments in Figure 7. In these experiments, BP equations are solved exactly for a given RHM starting with the initialisation of Equation 7. Our theory perfectly captures the probability of reconstruction for the input nodes and the class. Moreover, Figure 14 in Appendix B shows that our theory predicts the probabilities of reconstruction of latent nodes at all layers.

Experiment on CNN’s activations Similarly to our experiment on the ConvNeXt in Section 2, we investigate how the hidden representation of a model trained to classify the RHM changes when its input is denoised starting from a corruption noise ϵ . We consider an instantiation of the RHM with $L = 7$, $s = 2$, $v = 16$, and $m = 4$. First, we train a convolutional neural network with $L = 7$ layers, matching the tree structure of the model, with $n = 300k$ training examples up to interpolation. The resulting architecture has 99.2% test accuracy. To sample new data from noisy

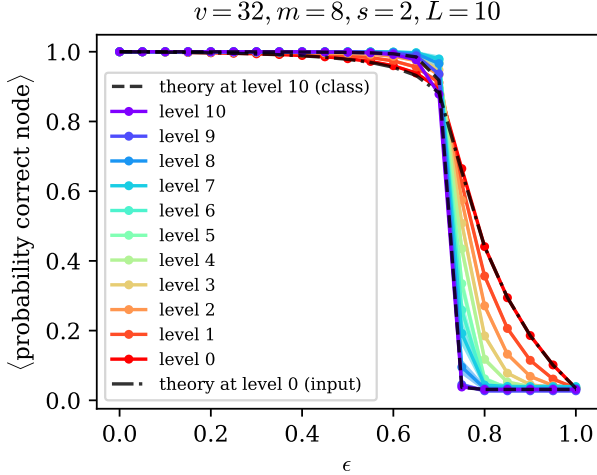


Figure 7. Probability that the latent has not changed in the denoising process, corresponding to the largest marginal probability computed by BP, for varying ϵ . Data for the RHM with $v = 32, m = 8, s = 2, L = 10$. Each level of the tree, indicated in the legend, is represented with a different colour. The black dashed lines are our mean-field theoretical predictions, which show excellent agreement with the experiments. In particular, the inversion between the curves for the top and bottom levels at the phase transition can be observed.

observations of held-out data, we start by sampling the root using the marginal probability computed with BP. Then, we update the beliefs and the marginals conditioning on the sampled class, and sample one latent variable at layer $L - 1$. We iterate this procedure node-by-node, descending the tree until we obtain a sampled configuration at the bottom layer (Mezard & Montanari, 2009). For each corrupting noise ϵ and each layer of the CNN, we compute the cosine similarity between post-activations for the initial and generated configurations. Figure 8 shows the obtained curves. Remarkably, we observe the same qualitative behaviour as in Figure 7, ultimately explaining the empirical observation of Figure 2.

6. Conclusions

We have argued that reversing time in denoising diffusion models opens a window on the compositional nature of data. For synthetic hierarchical generative data models, low-level features can already change at small times, but the class remains most often the same. At larger times, a phase transition is found where the probability of remaining in the same class suddenly drops to random chance. Yet, low-level features identical to those of the initial sample can persist and compose the new sample. Strikingly, the same results are found for ImageNet. These observations may thus be more general, and testing them in text datasets, using diffusion language models (He et al., 2022), is an interesting venue for future work.

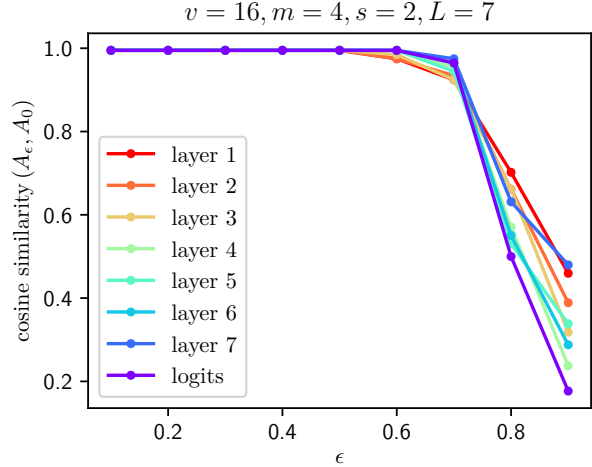


Figure 8. Cosine similarity between the post-activations following every layer of a deep CNN trained on the RHM ($v = 16, m = 4, s = 2, L = 7$) for the starting and sampled data. Each layer of the architecture, indicated in the legend, is represented with a different colour. The curves showcase the same inversion predicted by our theory (cf. Figure 7).

The interplay between the hierarchy in feature space and in time revealed here may help understand the puzzling success of diffusion models, including the number of data needed to train such methods, or why they can generalise and not simply memorise the empirical distribution on which they were trained (Somepalli et al., 2022; Carlini et al., 2023; Yoon et al., 2023). More generally, our results put forward hierarchical generative models as tools to understand open questions for other methods, ranging from the emergence of new skills by the composition of more elementary ones in self-supervised learning to that of transferable representations in supervised or contrastive learning.

Impact statement

This paper presents work whose goal is to advance the field of Machine Learning. There are many potential societal consequences of our work, none of which we feel must be specifically highlighted here.

Acknowledgements

We thank Francesco Cagnetta and Umberto Maria Tomasini for the helpful discussions. This work was supported by a grant from the Simons Foundation (#454953 Matthieu Wyart).

References

Allen-Zhu, Z. and Li, Y. Backward feature correction: How deep learning performs deep learning. *arXiv preprint arXiv:2001.04413*, 2020.

- Bach, F. Breaking the curse of dimensionality with convex neural networks. *The Journal of Machine Learning Research*, 18(1):629–681, 2017.
- Betker, J., Goh, G., Jing, L., Brooks, T., Wang, J., Li, L., Ouyang, L., Zhuang, J., Lee, J., Guo, Y., et al. Improving image generation with better captions. *Computer Science*. <https://cdn.openai.com/papers/dall-e-3.pdf>, 2(3), 2023.
- Biroli, G. and Mézard, M. Generative diffusion in very large dimensions. *arXiv preprint arXiv:2306.03518*, 2023.
- Block, A., Mroueh, Y., and Rakhlin, A. Generative modeling with denoising auto-encoders and langevin sampling. *arXiv preprint arXiv:2002.00107*, 2020.
- Cagnetta, F., Petrini, L., Tomasini, U. M., Favero, A., and Wyart, M. How deep neural networks learn compositional data: The random hierarchy model. *arXiv preprint arXiv:2307.02129*, 2023.
- Carlini, N., Hayes, J., Nasr, M., Jagielski, M., Sehwag, V., Tramèr, F., Balle, B., Ippolito, D., and Wallace, E. Extracting training data from diffusion models. In *32nd USENIX Security Symposium (USENIX Security 23)*, pp. 5253–5270, 2023.
- Chen, M., Huang, K., Zhao, T., and Wang, M. Score approximation, estimation and distribution recovery of diffusion models on low-dimensional data. *arXiv preprint arXiv:2302.07194*, 2023.
- Cui, H., Krzakala, F., Vanden-Eijnden, E., and Zdeborová, L. Analysis of learning a flow-based generative model from limited sample complexity. *arXiv preprint arXiv:2310.03575*, 2023.
- De Bortoli, V. Convergence of denoising diffusion models under the manifold hypothesis. *arXiv preprint arXiv:2208.05314*, 2022.
- DeGiuli, E. Random language model. *Physical Review Letters*, 122(12):128301, 2019.
- Dhariwal, P. and Nichol, A. Diffusion models beat gans on image synthesis. *Advances in neural information processing systems*, 34:8780–8794, 2021.
- He, K., Zhang, X., Ren, S., and Sun, J. Deep Residual Learning for Image Recognition. *IEEE Conference on Computer Vision and Pattern Recognition (CVPR)*, pp. 770–778, June 2016. doi: 10.1109/CVPR.2016.90.
- He, Z., Sun, T., Wang, K., Huang, X., and Qiu, X. Diffusionbert: Improving generative masked language models with diffusion models. *arXiv preprint arXiv:2211.15029*, 2022.
- Ho, J., Jain, A., and Abbeel, P. Denoising diffusion probabilistic models. *Advances in neural information processing systems*, 33:6840–6851, 2020.
- Kadkhodaie, Z., Guth, F., Mallat, S., and Simoncelli, E. P. Learning multi-scale local conditional probability models of images. *arXiv preprint arXiv:2303.02984*, 2023.
- LeCun, Y., Bengio, Y., and Hinton, G. Deep learning. *Nature*, 521(7553):436, 2015.
- Liu, Z., Mao, H., Wu, C.-Y., Feichtenhofer, C., Darrell, T., and Xie, S. A convnet for the 2020s. In *Proceedings of the IEEE/CVF conference on computer vision and pattern recognition*, pp. 11976–11986, 2022.
- Luxburg, U. v. and Bousquet, O. Distance-based classification with lipschitz functions. *The Journal of Machine Learning Research*, 5(Jun):669–695, 2004.
- Malach, E. and Shalev-Shwartz, S. A provably correct algorithm for deep learning that actually works. *arXiv preprint arXiv:1803.09522*, 2018.
- Malach, E. and Shalev-Shwartz, S. The implications of local correlation on learning some deep functions. *Advances in Neural Information Processing Systems*, 33:1322–1332, 2020.
- Mei, S. and Wu, Y. Deep networks as denoising algorithms: Sample-efficient learning of diffusion models in high-dimensional graphical models. *arXiv preprint arXiv:2309.11420*, 2023.
- Mezard, M. and Montanari, A. *Information, physics, and computation*. Oxford University Press, 2009.
- Mossel, E. Reconstruction on trees: beating the second eigenvalue. *The Annals of Applied Probability*, 11(1): 285–300, 2001.
- Mossel, E. Deep learning and hierarchical generative models. *arXiv preprint arXiv:1612.09057*, 2016.
- Nichol, A. Q. and Dhariwal, P. Improved denoising diffusion probabilistic models. In *International Conference on Machine Learning*, pp. 8162–8171. PMLR, 2021.
- Okawa, M., Lubana, E. S., Dick, R. P., and Tanaka, H. Compositional abilities emerge multiplicatively: Exploring diffusion models on a synthetic task. *arXiv preprint arXiv:2310.09336*, 2023.
- Oko, K., Akiyama, S., and Suzuki, T. Diffusion models are minimax optimal distribution estimators. *arXiv preprint arXiv:2303.01861*, 2023.
- Olah, C., Cammarata, N., Schubert, L., Goh, G., Petrov, M., and Carter, S. Zoom in: An introduction to circuits. *Distill*, 5(3):e00024–001, 2020.

- Poggio, T., Mhaskar, H., Rosasco, L., Miranda, B., and Liao, Q. Why and when can deep-but not shallow-networks avoid the curse of dimensionality: a review. *International Journal of Automation and Computing*, 14(5):503–519, 2017.
- Rombach, R., Blattmann, A., Lorenz, D., Esser, P., and Ommer, B. High-resolution image synthesis with latent diffusion models. In *Proceedings of the IEEE/CVF conference on computer vision and pattern recognition*, pp. 10684–10695, 2022.
- Rozenberg, G. and Salomaa, A. *Handbook of Formal Languages*. Springer, January 1997. doi: 10.1007/978-3-642-59126-6.
- Schmidt-Hieber, J. Nonparametric regression using deep neural networks with relu activation function. *The Annals of Statistics*, 48(4):1875–1897, 2020.
- Shah, K., Chen, S., and Klivans, A. Learning mixtures of gaussians using the ddpm objective. *arXiv preprint arXiv:2307.01178*, 2023.
- Shalev-Shwartz, S., Shamir, O., and Shammah, S. Failures of gradient-based deep learning. In *International Conference on Machine Learning*, pp. 3067–3075. PMLR, 2017.
- Sohl-Dickstein, J., Weiss, E., Maheswaranathan, N., and Ganguli, S. Deep unsupervised learning using nonequilibrium thermodynamics. In *International conference on machine learning*, pp. 2256–2265. PMLR, 2015.
- Somepalli, G., Singla, V., Goldblum, M., Geiping, J., and Goldstein, T. Diffusion art or digital forgery. *Investigating Data Replication in Diffusion Models*, 2022.
- Song, Y. and Ermon, S. Generative modeling by estimating gradients of the data distribution. *Advances in neural information processing systems*, 32, 2019.
- Song, Y., Sohl-Dickstein, J., Kingma, D. P., Kumar, A., Ermon, S., and Poole, B. Score-based generative modeling through stochastic differential equations. *arXiv preprint arXiv:2011.13456*, 2020.
- TorchVision maintainers and contributors. Torchvision: Pytorch’s computer vision library. <https://github.com/pytorch/vision>, 2016.
- Yoon, T., Choi, J. Y., Kwon, S., and Ryu, E. K. Diffusion probabilistic models generalize when they fail to memorize. In *ICML 2023 Workshop on Structured Probabilistic Inference & Generative Modeling*, 2023.
- Yuan, H., Huang, K., Ni, C., Chen, M., and Wang, M. Reward-directed conditional diffusion: Provable distribution estimation and reward improvement. *arXiv preprint arXiv:2307.07055*, 2023.
- Zeiler, M. D. and Fergus, R. Visualizing and understanding convolutional networks. In *Computer Vision – ECCV 2014*, Lecture Notes in Computer Science, pp. 818–833, 2014.

A. Belief Propagation initialization for the denoising of the RHM

As discussed in Section 4, we define the diffusion process for the input variable $X_i^{(0)}$ in the space \mathbb{R}^v . In particular, its value $x(t)$ at time t is

$$x(t) = \sqrt{\alpha_t}x(0) + \sqrt{1 - \alpha_t}\eta, \quad (9)$$

with $\eta \sim \mathcal{N}(0, \mathbb{I}_v)$ and $x(0)$ its starting value at time t , which is a one-hot-encoding vector of the form $x(0) = e_\mu$. Given the value $x(t)$, the conditional probabilities for the values of $x(0)$ are given by Bayes rule

$$p(x(0) = e_\mu | x(t)) = \frac{p(x(t) | x(0) = e_\mu) p(x(0) = e_\mu)}{\sum_\lambda p(x(t) | x(0) = e_\lambda) p(x(0) = e_\lambda)}. \quad (10)$$

The prior probabilities on $x(0)$ are taken to be uniform over the alphabet, i.e., $p(x(0) = e_\lambda) = 1/v$, $\forall \lambda$, while $p(x(t) | x(0) = e_\mu)$ is given by the diffusion process of Eq. 9:

$$\begin{aligned} p(x(t) | x(0) = e_\mu) &= C_t \exp \left[-\frac{1}{2(1 - \alpha_t)} \sum_\gamma (x_\gamma(t) - \sqrt{\alpha_t}e_\mu)^2 \right] = \\ &= C_t \exp \left[-\frac{(\|x(t)\|^2 - \alpha_t)}{2(1 - \alpha_t)} \right] \exp \left[\frac{\sqrt{\alpha_t}}{1 - \alpha_t} x_\mu(t) \right], \end{aligned} \quad (11)$$

where C_t is the normalization constant. Putting Eq. 11 into Eq. 10, we obtain

$$p(x(0) = e_\mu | x(t)) = \frac{1}{Z} e^{\frac{\sqrt{\alpha_t}}{1 - \alpha_t} x_\mu(t)}, \quad (12)$$

with $Z = \sum_{\lambda=1}^v e^{\frac{\sqrt{\alpha_t}}{1 - \alpha_t} x_\lambda(t)}$.

B. Belief Propagation equations

Given a factor tree-graph, the Belief Propagation (BP) equations compute iteratively the messages going from the variable nodes to the factor nodes and vice-versa, starting from the initialization conditions at the leaves and root of the tree-graph (Mezard & Montanari, 2009). For the generative model defined in Sec. 3, the leaves correspond to the variables at the bottom layer while the root is the class variable at the top of the hierarchy. Each rule, connecting variables at different layers, corresponds to a factor node. The BP messages that flow from the variable nodes to the factor nodes, therefore, correspond to upward messages, while those going from factor nodes to variables correspond to downward messages (Fig. 9).

To each variable node $X_i^{(\ell)}$ at level ℓ , we associate the upward messages $\nu_\uparrow^{(\ell)}$ and downward messages $\nu_\downarrow^{(\ell)}$, one for each possible value of the alphabet it can take. To simplify the notation, here we consider how messages propagate from one level to the other and we call Y the variable corresponding to the higher level and $X_{i=1, \dots, s}$ the lower level ones connected to it. The factor node connecting them is such that, for each possible association $y \rightarrow x_1, \dots, x_s$, it takes values

$$\psi^{(\ell)}(y, x_1, \dots, x_s) = \begin{cases} 1, & \text{if } y \rightarrow (x_1, \dots, x_s) \text{ is a rule at layer } \ell \\ 0, & \text{otherwise.} \end{cases}$$

The BP upward and downward iterations are defined as follows.

- Upward iteration:

$$\tilde{\nu}_\uparrow^{(\ell+1)}(y) = \sum_{x_1, \dots, x_s \in \mathcal{A}^{\otimes s}} \psi^{(\ell+1)}(y, x_1, \dots, x_s) \prod_{i=1}^s \nu_\uparrow^{(\ell)}(x_i), \quad (13)$$

$$\nu_\uparrow^{(\ell)}(y) = \frac{\tilde{\nu}_\uparrow^{(\ell)}(y)}{\sum_{y'} \tilde{\nu}_\uparrow^{(\ell)}(y')}. \quad (14)$$

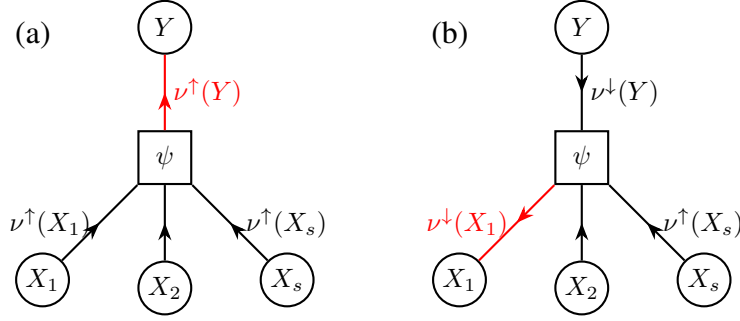


Figure 9. Factor tree-graph connecting the higher-level feature Y to the lower-level features $X_{i=1,\dots,s}$ according to the rules ψ . The upward messages $\nu^\uparrow(y)$ are computed from the upward messages $\nu^\uparrow(x_i)$ coming from the nodes X_i , connected to Y through the rule ψ (panel (a)). The downward messages $\nu^\downarrow(x_1)$, instead, are computed from both the downward messages $\nu^\downarrow(y)$ coming from Y and the upward messages $\nu^\uparrow(x_i)$ coming from the nodes $X_{i=2,\dots,s}$, connected to X_1 through the rule ψ (panel (b)).

- Downward iteration:

$$\tilde{\nu}_\downarrow^{(\ell)}(x_1) = \sum_{\substack{x_2, \dots, x_s \in \mathcal{A}^{\otimes(s-1)} \\ y \in \mathcal{A}}} \psi^{(\ell+1)}(y, x_1, \dots, x_s) \nu_\downarrow^{(\ell+1)}(y) \prod_{i=2}^s \nu_\uparrow^{(\ell)}(x_i) \quad (15)$$

$$\nu_\downarrow^{(l)}(x) = \frac{\tilde{\nu}_\downarrow^{(\ell)}(x)}{\sum_{x'} \tilde{\nu}_\downarrow^{(\ell)}(x')}. \quad (16)$$

$\nu_\uparrow^{(\ell)}(y)$ and $\nu_\downarrow^{(\ell)}(x)$ are fluctuating quantities that depend on the position of the node.

B.1. ϵ -process

In this process, we consider a reference configuration at the leaves variables $X_i^{(0)} = \bar{x}_i$ that we would like to reconstruct, given a noisy observation of it. As a result of this noise addition, our belief in the correct sequence is corrupted by $\epsilon \in [0, 1]$:

$$\begin{cases} X_i^{(0)} = \bar{x}_i & \text{with belief } 1 - \epsilon \\ X_i^{(0)} \text{ uniform over alphabet} & \text{with belief } \epsilon. \end{cases} \quad (17)$$

Therefore, the initialization condition of the upward BP messages at a leaf node $X_i^{(0)}$ is

$$\begin{cases} \nu_\uparrow(\bar{x}_i) &= 1 - \epsilon + \epsilon/v, \\ \nu_\uparrow(x_i \neq \bar{x}_i) &= \epsilon/v, \end{cases} \quad (18)$$

where v is the corresponding alphabet size.

The initialization condition at the root node $X^{(L)}$, that corresponds to the messages $\nu_\downarrow^{(L)}$ for that node, is uniform over the alphabet \mathcal{A} , so that the algorithm has no bias on any specific class.

B.1.1. UPWARD ITERATION

We consider the upward iteration when going from the bottom layer to the one above it. Let X_1, \dots, X_s denote a tuple at the bottom level which is associated with the reference values \bar{x}_i . This tuple is connected to the higher level variable Y via a set of rules ψ (Fig. 9). According to ψ , the association from the high-level feature to the reference low-level sequence $\bar{x}_1, \dots, \bar{x}_s$ is given by

$$\bar{y} \rightarrow \bar{x}_1, \dots, \bar{x}_s.$$

We call $\Delta_{\mathbf{w}, \mathbf{z}}$ the Hamming distance between two sequences $\mathbf{w} = [w_1, \dots, w_s]$, $\mathbf{z} = [z_1, \dots, z_s]$ of length s .

From Eq. 18, at the bottom layer, the belief in a sequence $\mathbf{x} = [x_1, \dots, x_s]$ with $\Delta_{\mathbf{x}, \bar{\mathbf{x}}} = k \in \{0, \dots, s\}$ from $\bar{\mathbf{x}} =$

$[\bar{x}_1, \dots, \bar{x}_s]$ is

$$\mathcal{B}(k) = \left(\frac{\epsilon}{v}\right)^k \left(1 - \epsilon + \frac{\epsilon}{v}\right)^{s-k} \quad (19)$$

The non-normalized upward messages for the variable Y are given by:

$$\tilde{\nu}_\uparrow(y) = \sum_{x_1, \dots, x_s} \psi(y, x_1, \dots, x_s) \prod_{i=1}^s \nu_\uparrow(x_i) = \sum_{\mathbf{x} \in \mathcal{S}} \psi(y, \mathbf{x}) \mathcal{B}(\Delta_{\mathbf{x}, \bar{\mathbf{x}}}), \quad (20)$$

where we are using the short-hand notation $\psi(y, x_1, \dots, x_s) = \psi(y, \mathbf{x})$ and we have restricted the sum over the set \mathcal{S} of sequences \mathbf{x} that appear in the possible rules $y \rightarrow x_1, \dots, x_s$. In fact, if $\mathbf{x} \notin \mathcal{S}$, then $\psi(y, \mathbf{x}) = 0$.

For $\mathbf{x} \in \mathcal{S}$, the factor $\psi(y, \mathbf{x})$ is such that:

- if $\Delta_{\mathbf{x}, \bar{\mathbf{x}}} = 0$:

$$\begin{cases} \psi(\bar{y}, \bar{x}_1, \dots, \bar{x}_s) = 1, \\ \psi(y, \bar{x}_1, \dots, \bar{x}_s) = 0, \quad y \neq \bar{y}. \end{cases} \quad (21)$$

- if $\Delta_{\mathbf{x}, \bar{\mathbf{x}}} > 0$:

$$\begin{cases} \psi(\tilde{y}, x_1, \dots, x_s) = 1, & \text{for some } \tilde{y} \text{ independent of } \bar{y} \\ \psi(y, x_1, \dots, x_s) = 0, & y \neq \tilde{y}. \end{cases} \quad (22)$$

We can decompose Eq. 20 as

$$\tilde{\nu}_\uparrow(y) = \delta_{y, \bar{y}} \mathcal{B}(0) + \sum_{k=1}^s \mathcal{B}(k) \left[\sum_{\substack{\mathbf{x} \in \mathcal{S} \\ \Delta_{\mathbf{x}, \bar{\mathbf{x}}} = k}} \psi(y, \mathbf{x}) \right]. \quad (23)$$

Annealed average ψ is a random quantity and we want to compute the average message $\langle \tilde{\nu}_\uparrow(y) \rangle_\psi$ over the possible realizations of ψ . We can decompose the selection of the rules in two steps: sampling the set of $mv - 1$ sequences $\{\mathbf{x}, \mathbf{x} \neq \bar{\mathbf{x}}\}$ and then associating the v higher-level features y to them. Therefore, for a generic quantity A , we indicate the average over the rules realization $\langle A \rangle_\psi$ as $\langle \langle A \rangle_{\{y\} \leftarrow \{\mathbf{x}\}} \rangle_{\mathcal{S}}$, where $\langle \dots \rangle_{\mathcal{S}}$ is the average over the sequence sampling and $\langle \dots \rangle_{\{y\} \leftarrow \{\mathbf{x}\}}$ is the average over the $y \leftarrow \mathbf{x}$ associations:

$$\langle \tilde{\nu}_\uparrow(y) \rangle_\psi = \delta_{y, \bar{y}} \mathcal{B}(0) + \sum_{k=1}^s \mathcal{B}(k) \langle \langle \sum_{\substack{\mathbf{x} \in \mathcal{S} \\ \Delta_{\mathbf{x}, \bar{\mathbf{x}}} = k}} \psi(y, \mathbf{x}) \rangle_{\{y\} \leftarrow \{\mathbf{x}\}} \rangle_{\mathcal{S}} \quad (24)$$

Since for each sequence $\mathbf{x} \neq \bar{\mathbf{x}}$ the association $y \leftarrow \mathbf{x}$ is done randomly, independently of $\Delta_{\mathbf{x}, \bar{\mathbf{x}}}$, then from Eq. 22, we have $\langle \psi(y, \mathbf{x}) \rangle_{\{y\} \leftarrow \{\mathbf{x}\}} \simeq 1/v$. More precisely, since we have associated the reference sequence $\bar{\mathbf{x}}$ to \bar{y} :

$$\overline{\psi_y} = \langle \psi(y, \mathbf{x}) \rangle_{\{y\} \leftarrow \{\mathbf{x}\}} = \frac{m-1}{mv-1} \delta_{y, \bar{y}} + \frac{m}{mv-1} (1 - \delta_{y, \bar{y}}). \quad (25)$$

Therefore:

$$\begin{aligned} \langle \tilde{\nu}_\uparrow(y) \rangle_\psi &= \delta_{y, \bar{y}} \mathcal{B}(0) + \overline{\psi_y} \sum_{k=1}^s \mathcal{B}(k) \langle \sum_{\substack{\mathbf{x} \in \mathcal{S} \\ \Delta_{\mathbf{x}, \bar{\mathbf{x}}} = k}} 1 \rangle_{\mathcal{S}} = \\ &= \delta_{y, \bar{y}} \mathcal{B}(0) + \overline{\psi_y} \sum_{k=1}^s \mathcal{B}(k) \langle n_k \rangle_{\mathcal{S}}, \end{aligned} \quad (26)$$

where n_k is the number of sequences $\mathbf{x} \in \mathcal{S}$ having Hamming distance $\Delta_{\mathbf{x}, \bar{\mathbf{x}}} = k$ from $\bar{\mathbf{x}}$. Since the sequences are sampled randomly, the numbers n_1, \dots, n_s are distributed according to a multivariate hyper-geometric distribution,

$$P(n_1, \dots, n_s) = \frac{\prod_{k=1}^s \binom{s}{k} \binom{v-1}{n_k}}{\binom{v^s-1}{mv-1}}, \quad (27)$$

which gives the averages

$$\langle n_k \rangle_{\mathcal{S}} = \frac{mv-1}{v^s-1} \binom{s}{k} (v-1)^k = f \binom{s}{k} (v-1)^k, \quad (28)$$

with

$$f = \frac{mv-1}{v^s-1}. \quad (29)$$

Therefore:

$$\langle \tilde{\nu}_{\uparrow}(y) \rangle_{\psi} = \delta_{y, \bar{y}} \mathcal{B}(0) + f \overline{\psi}_y \sum_{k=1}^s \mathcal{B}(k) \binom{s}{k} (v-1)^k. \quad (30)$$

From the beliefs Eq. 19, we see that

$$\sum_{k=1}^s \mathcal{B}(k) \binom{s}{k} (v-1)^k = \sum_{k=1}^s \binom{s}{k} (v-1)^k \left(\frac{\epsilon}{v}\right)^k \left(1 - \epsilon + \frac{\epsilon}{v}\right)^{s-k} = \left[1 - \left(1 - \epsilon + \frac{\epsilon}{v}\right)^s\right] = 1 - \mathcal{B}(0), \quad (31)$$

which gives

$$\langle \tilde{\nu}_{\uparrow}(y) \rangle_{\psi} = \delta_{y, \bar{y}} \mathcal{B}(0) + f \overline{\psi}_y [1 - \mathcal{B}(0)]. \quad (32)$$

The normalization constant is:

$$\langle Z_{\uparrow} \rangle_{\psi} = \sum_y \langle \tilde{\nu}_{\uparrow}(y) \rangle_{\psi} = \mathcal{B}(0) + f [1 - \mathcal{B}(0)]. \quad (33)$$

Finally, we obtain the average belief for Y

$$\langle \nu_{\uparrow}(y) \rangle_{\psi} = \frac{\langle \tilde{\nu}_{\uparrow}(y) \rangle_{\psi}}{\langle Z_{\uparrow} \rangle_{\psi}} = \frac{\delta_{y, \bar{y}} \mathcal{B}(0) + f \overline{\psi}_y [1 - \mathcal{B}(0)]}{\mathcal{B}(0) + f [1 - \mathcal{B}(0)]} \quad (34)$$

We have that:

- for $y = \bar{y}$

$$\langle \nu_{\uparrow}(\bar{y}) \rangle_{\psi} = \frac{\mathcal{B}(0) + f \frac{m-1}{mv-1} [1 - \mathcal{B}(0)]}{\mathcal{B}(0) + f [1 - \mathcal{B}(0)]}, \quad (35)$$

- for $y \neq \bar{y}$

$$\langle \nu_{\uparrow}(y) \rangle_{\psi} = f \frac{m}{mv-1} \frac{1 - \mathcal{B}(0)}{\mathcal{B}(0) + f [1 - \mathcal{B}(0)]}. \quad (36)$$

Iterating over layers The average messages in Eqs. 35, 36 are of two kinds: one for the reference feature \bar{y} and another for the others $y \neq \bar{y}$, and they both depend on the previous beliefs through $\mathcal{B}(0) = \left(1 - \epsilon + \frac{\epsilon}{v}\right)^s$. Therefore, the average messages at the higher level have the same structure as those at the lower level Eq. 18. We can then define a new ϵ' :

$$1 - \epsilon' + \frac{\epsilon'}{v} = \frac{\left(1 - \epsilon + \frac{\epsilon}{v}\right)^s + f \frac{m-1}{mv-1} [1 - \left(1 - \epsilon + \frac{\epsilon}{v}\right)^s]}{\left(1 - \epsilon + \frac{\epsilon}{v}\right)^s + f [1 - \left(1 - \epsilon + \frac{\epsilon}{v}\right)^s]} \quad (37)$$

or, equivalently,

$$p' = \frac{p^s + f \frac{m-1}{mv-1} (1 - p^s)}{p^s + f (1 - p^s)} = F(p) \quad (38)$$

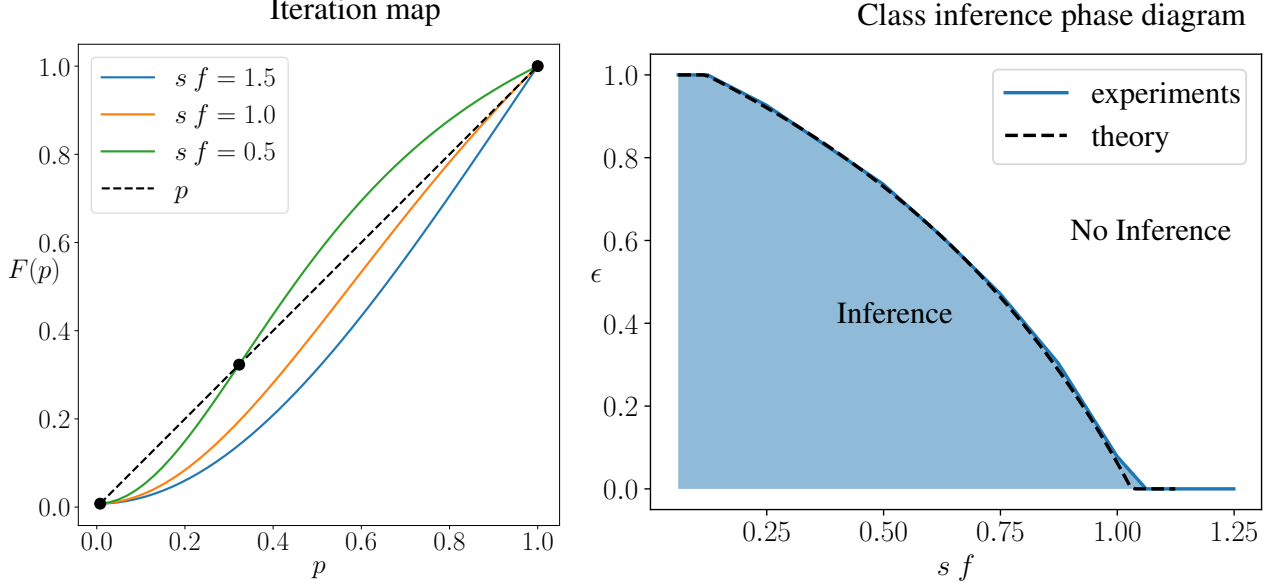


Figure 10. *Left panel: Iteration map of Eq. 38.* For $sf > 1$, there are only two fixed points $p = F(p)$ corresponding to $p_1 = 1$ (repulsive) and $p_2 = 1/v$ (attractive). For $sf < 1$, there is another (repulsive) fixed point at finite p^* , $1/v < p^* < 1$, separating p_1 and p_2 (both attractive). *Right panel: Phase diagram for inferring the class node using the upwards iteration of BP.* When $sf < 1$, BP can infer the class of the datum if $\epsilon < \epsilon^*(sf)$. This transition is well predicted by $p^* = 1 - \epsilon^* + \epsilon^*/v$, with $p^* = F(p^*)$ from Eq. 38. Experimental data for $v = 32$, $s = 2$, $L = 10$.

with $p' = 1 - \epsilon' + \epsilon'/v$ and $p = 1 - \epsilon + \epsilon/v$. The derivative of $F(p)$ with respect to p is given by¹

$$F'(p) = \frac{m(v-1)}{mv-1} \frac{f s p^{s-1}}{[p^s + f(1-p^s)]^2} = f s \frac{p^{s-1}}{[p^s + f(1-p^s)]^2} + \mathcal{O}\left(\frac{1}{v}\right) \quad (39)$$

We can extend the tree in Fig. 9 iteratively to higher levels of the hierarchy, where the variables Y take the place of the variables X_i and so on.

The iteration Eq. 38 has fixed points $p = 1$ (corresponding to $\epsilon = 0$) or $p = 1/v$ (corresponding to $\epsilon = 1$). An additional repulsive fixed point at finite p appears if

$$F'(1) < 1, \quad (40)$$

that is

$$\frac{m(v-1)}{mv-1} f s < 1 \quad \Rightarrow \quad f s < 1 + \frac{1 - 1/m}{v - 1} \quad (41)$$

$$\Rightarrow \quad f s < 1 + \mathcal{O}\left(\frac{1}{v}\right). \quad (42)$$

B.1.2. DOWNWARD ITERATION

We consider the downward process when we try reconstructing the reference association $\bar{y} \rightarrow \bar{x}_1, \dots, \bar{x}_s$ from higher-level variable Y to the corresponding lower-level tuple X_1, \dots, X_s , via the set of rules ψ . We consider the downward message

received by the variable X_1 (Fig. 9):

$$\begin{aligned}\tilde{\nu}_\downarrow(x_1) &= \sum_{\substack{x_2, \dots, x_s \in \mathcal{A}^{\otimes(s-1)} \\ y \in \mathcal{A}}} \psi(y, x_1, \dots, x_s) \nu_\downarrow(y) \prod_{i=2}^s \nu_\uparrow(x_i) = \\ &= \delta_{x_1, \bar{x}_1} \nu_\downarrow(\bar{y}) \prod_{i=2}^s \nu_\uparrow(\bar{x}_i) + \sum_y \nu_\downarrow(y) \sum_{\substack{x_2, \dots, x_s \\ \mathbf{x} \in \mathcal{S}, \Delta_{\mathbf{x}, \bar{\mathbf{x}}} > 0}} \psi(y, \mathbf{x}) \prod_{i=2}^s \nu_\uparrow(x_i)\end{aligned}\quad (43)$$

Annealed average To study the iteration of Eq. 43 analytically, we compute the average message $\langle \tilde{\nu}_\downarrow(x_1) \rangle_\psi$ over the realizations of the random rules ψ as done in Sec. B.1.2 for the upward iteration.

We call n_{x_1} the number of sequences, having $X_1 = x_1$, that have been sampled by the choice of the rules. The numbers n_{x_1} are distributed according to a multivariate hyper-geometric distribution,

$$P(\{n_{x_1}\}_{x_1 \in \mathcal{A}}) = \frac{\binom{v^{s-1}-1}{n_{\bar{x}_1}} \prod_{\bar{x}_1 \in \mathcal{A} \setminus \bar{x}_1} \binom{v^{s-1}}{n_{\bar{x}_1}}}{\binom{v^s-1}{mv-1}}, \quad (44)$$

which gives averages

$$\langle n_{\bar{x}_1} \rangle = \frac{mv-1}{v^s-1} (v^{s-1}-1) = f(v^{s-1}-1), \quad (45)$$

$$\langle n_{\bar{x}_1 \neq \bar{x}_1} \rangle = \frac{mv-1}{v^s-1} v^{s-1} = f v^{s-1}. \quad (46)$$

Averaging the downward messages over the choices of rules ψ , we obtain:

- for $x_1 \neq \bar{x}_1$:

$$\begin{aligned}\langle \tilde{\nu}_\downarrow(x_1) \rangle_\psi &= \sum_y \nu_\downarrow(y) \langle \sum_{\substack{x_2, \dots, x_s \\ \mathbf{x} \in \mathcal{S}}} \langle \psi(y, \mathbf{x}) \rangle_{\{y\} \leftarrow \{\mathbf{x}\}} \prod_{i=2}^s \nu_\uparrow(x_i) \rangle_{\mathcal{S}} = \\ &= \frac{m - \nu_\downarrow(\bar{y})}{mv-1} \langle \delta_{\mathbf{x} \in \mathcal{S}} \rangle_{\mathcal{S}} \prod_{i=2}^s \sum_{x_i} \nu_\uparrow(x_i) = \frac{m - \nu_\downarrow(\bar{y})}{mv-1} f = \\ &= \frac{m - \nu_\downarrow(\bar{y})}{mv-1} f,\end{aligned}\quad (47)$$

where $\langle \delta_{\mathbf{x} \in \mathcal{S}} \rangle_{\mathcal{S}} = \frac{\langle n_{x_1 \neq \bar{x}_1} \rangle}{v^{s-1}-1}$;

- for $x_1 = \bar{x}_1$:

$$\begin{aligned}\langle \tilde{\nu}_\downarrow(\bar{x}_1) \rangle_\psi &= \nu_\downarrow(\bar{y}) \prod_{i=2}^s \nu_\uparrow(\bar{x}_i) + \sum_y \nu_\downarrow(y) \langle \sum_{\substack{x_2, \dots, x_s \\ \mathbf{x} \in \mathcal{S}, \mathbf{x} \neq \bar{\mathbf{x}}}} \langle \psi(y, \mathbf{x}) \rangle_{\{y\} \leftarrow \{\mathbf{x}\}} \prod_{i=2}^s \nu_\uparrow(x_i) \rangle_{\mathcal{S}} = \\ &= \nu_\downarrow(\bar{y}) \prod_{i=2}^s \nu_\uparrow(\bar{x}_i) + \frac{m - \nu_\downarrow(\bar{y})}{mv-1} \langle \delta_{\mathbf{x} \in \mathcal{S}} \rangle_{\mathcal{S}} \sum_{\substack{x_2, \dots, x_s \\ \mathbf{x} \in \mathcal{S}, \mathbf{x} \neq \bar{\mathbf{x}}}} \prod_{i=2}^s \nu_\uparrow(x_i) = \\ &= \nu_\downarrow(\bar{y}) \prod_{i=2}^s \nu_\uparrow(\bar{x}_i) + \frac{m - \nu_\downarrow(\bar{y})}{mv-1} f \left[1 - \prod_{i=2}^s \nu_\uparrow(\bar{x}_i) \right]\end{aligned}\quad (48)$$

where $\langle \delta_{\mathbf{x} \in \mathcal{S}} \rangle_{\mathcal{S}} = \frac{\langle n_{\bar{x}_1} \rangle}{v^{s-1}-1}$.

The normalization factor is

$$\langle Z_{\downarrow} \rangle_{\psi} = \sum_{x_1} \langle \tilde{\nu}_{\downarrow}(x_1) \rangle_{\psi} = \nu_{\downarrow}(\bar{y}) \prod_{i=2}^s \nu_{\uparrow}(\bar{x}_i) + f \frac{m - \nu_{\downarrow}(\bar{y})}{mv - 1} \left[1 - \prod_{i=2}^s \nu_{\uparrow}(\bar{x}_i) \right] + (v - 1) f \frac{m - \nu_{\downarrow}(\bar{y})}{mv - 1} \quad (49)$$

which gives the normalized average messages:

- for $x_1 = \bar{x}_1$

$$\langle \nu_{\downarrow}(\bar{x}_1) \rangle_{\psi} = \frac{\nu_{\downarrow}(\bar{y}) \prod_{i=2}^s \nu_{\uparrow}(\bar{x}_i) + f \frac{m - \nu_{\downarrow}(\bar{y})}{mv - 1} [1 - \prod_{i=2}^s \nu_{\uparrow}(\bar{x}_i)]}{\langle Z_{\downarrow} \rangle_{\psi}}; \quad (50)$$

- for $x_1 \neq \bar{x}_1$

$$\langle \nu_{\downarrow}(x_1) \rangle_{\psi} = f \frac{m - \nu_{\downarrow}(\bar{y})}{\langle Z_{\downarrow} \rangle_{\psi}}. \quad (51)$$

Iterating over layers As for the upward process, the average messages for the downward process are of two kinds, one for the correct value \bar{x}_1 and one for the other values $x_1 \neq \bar{x}_1$. To obtain a mean-field description of the BP process, we combine the average downward messages with the average upward ones, by substituting $\nu_{\uparrow}(\bar{x}_i) \rightarrow \langle \nu_{\uparrow}(\bar{x}_i) \rangle$ in Eq. 50. We use the notation

$$\langle \nu_{\uparrow}^{(\ell)}(\bar{x}_i) \rangle = p_{\uparrow}^{(\ell)}, \quad (52)$$

$$\langle \nu_{\downarrow}^{(\ell)}(\bar{x}_i) \rangle = p_{\downarrow}^{(\ell)}, \quad (53)$$

where the upwards and downwards beliefs $p_{\uparrow}^{(\ell)}, p_{\downarrow}^{(\ell)}$ in the correct value for the latent variable $X_i^{(\ell)}$ depend only on the layer ℓ and not on the specific position i inside the layer. Putting together Eqs. 38 and 50, we obtain

$$\begin{aligned} p_{\uparrow}^{(\ell+1)} &= F_{\uparrow}(p_{\uparrow}^{(\ell)}), \\ p_{\downarrow}^{(\ell)} &= F_{\downarrow}(p_{\downarrow}^{(\ell+1)}, p_{\uparrow}^{(\ell)}), \end{aligned} \quad (54)$$

with

$$F_{\uparrow}(p) = \frac{p^s + f \frac{m-1}{mv-1} (1 - p^s)}{p^s + f (1 - p^s)}, \quad (55)$$

$$F_{\downarrow}(q, p) = \frac{q p^{s-1} + f \frac{m-q}{mv-1} (1 - p^{s-1})}{q p^{s-1} + f \frac{m-q}{mv-1} (1 - p^{s-1}) + (v-1) f \frac{m-q}{mv-1}}, \quad (56)$$

and the initialization condition

$$p_{\uparrow}^{(0)} = 1 - \epsilon + \epsilon/v, \quad (57)$$

$$p_{\downarrow}^{(L)} = 1/v. \quad (58)$$

From $p_{\uparrow}^{(\ell)}$ and $p_{\downarrow}^{(\ell)}$, at layer ℓ , the average marginal probability of the correct value $p^{(\ell)}$ is given by

$$p^{(\ell)} = \frac{p_{\uparrow}^{(\ell)} p_{\downarrow}^{(\ell)}}{p_{\uparrow}^{(\ell)} p_{\downarrow}^{(\ell)} + \frac{(1-p_{\uparrow}^{(\ell)})(1-p_{\downarrow}^{(\ell)})}{v-1}}. \quad (59)$$

B.1.3. VALIDITY OF THE MEAN-FIELD THEORY

Due to the randomness of the production rules, the messages $\nu_{\uparrow}(x), \nu_{\downarrow}(x)$ are random variables which depend on the specific realization of the rules. Although their fluctuations are not captured by the averages computed in Eq. 54, we observe that

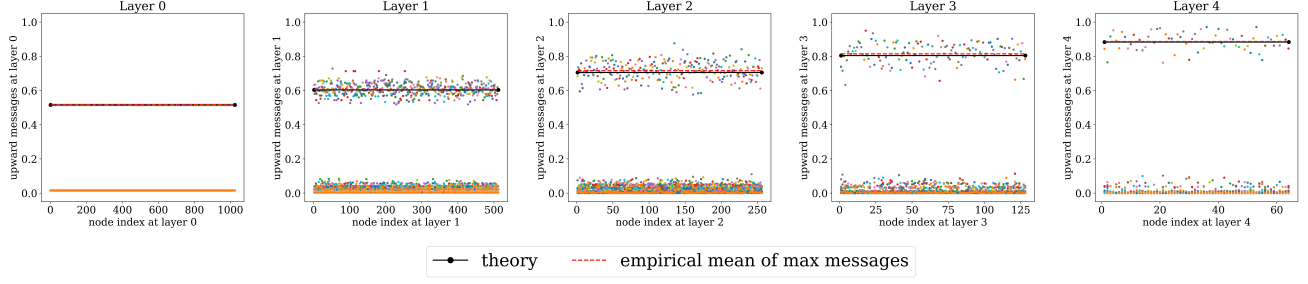


Figure 11. **Upward BP messages for layers 0 to 4** for $\epsilon = 0.5$, $v = 32$, $s = 2$, $L = 10$, $sf = 0.5$. Each node has v messages, one per possible feature. At the input layer (layer 0), messages have value $1 - \epsilon = 0.5$ or $\epsilon/v = 0.5/32$. Going upward, the values of the messages fluctuate, but they stay separated into two distinct groups: large messages (i.e., the most probable feature for each node) and small ones. The annealed mean-field computation (represented with a black line) captures well the mean value of the large messages (red dashed line).

$p_{\uparrow}^{(\ell)}$ and $p_{\downarrow}^{(\ell)}$ capture well the average behaviour of the messages at a given layer. In Fig. 11, the values of $\nu_{\uparrow}^{(\ell)}(X_i^{(\ell)})$ are reported for the bottom 5 levels of a Random Hierarchical Model with $L = 10$, $s = 2$, $v = 32$, $m = 8$, and noise level $\epsilon = 0.5$. At each layer ℓ , the index i of the nodes goes from 1 to $s^{L-\ell}$ and for each of them there are $v = 32$ messages $\nu_{\uparrow}^{(\ell)}$, one for each entry of the alphabet. At layer $\ell = 0$, the messages $\nu_{\uparrow}^{(0)}$ are initialized according to Eq. 18. After one iteration, at layer $\ell = 1$ we observe that the largest messages at each node, those corresponding to the most probable features x_i , are spread around some mean value that is well captured by the theoretical prediction of Eq. 54. We observe that also for the upper layers, the average behaviour of the largest messages is well captured by the theory.

The comparison between the theory and the BP algorithm for every ϵ is reported in the Figs. 12 and 13. The upward iteration is reported in Fig. 12 and shows an excellent agreement with the prediction of Eq. 54. In particular, going from the input layer $\ell = 0$ to the class variable $\ell = L$ ($L = 10$ in Fig. 12), the messages for the most probable features show a sharper transition at a threshold value ϵ^* , which corresponds to the phase transition of the theoretical iteration map in Eq. 38 when $L \rightarrow \infty$. The downward iteration in Fig. 13 shows that the theory also captures the trend in ϵ of the downward messages. However, for small values of ϵ , we observe that the messages have large fluctuations around their mean value. The reason for this behaviour is that, in the Random Hierarchical Model, there is a number m of synonyms (x_1, \dots, x_s) that codes for the same higher level feature y . Therefore, having perfect information on y and on x_2, \dots, x_s is not enough to perfectly reconstruct the value of x_1 , thereby resulting in large fluctuations of the messages at small noise level ϵ . This is different from the upward process where, having perfect information on (x_1, \dots, x_s) allows the perfect reconstruction of y . As a result, the messages in the upward process are more concentrated around their mean than the downward messages.

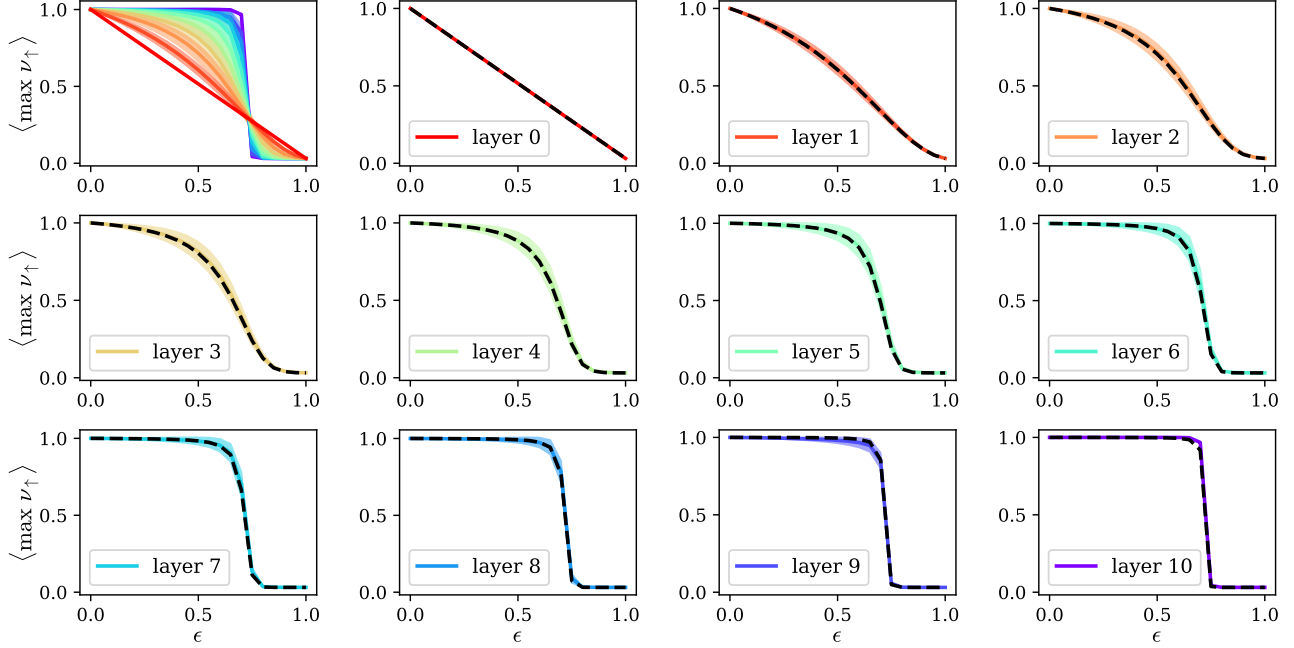


Figure 12. **Largest upward BP messages, averaged for each layer, for varying ϵ .** Data for the Random Hierarchical Model with $v = 32, s = 2, L = 10, sf = 0.5$. Each layer, indicated in the legend, is represented with a different colour and the black dashed line is the theoretical prediction from Eq. 54, which shows excellent agreement with the experiments. The top left panel represents all the layers together for comparison. Starting from the initialization $\nu_{\uparrow} = 1 - \epsilon + \epsilon/v$ at layer 0, we observe that the largest upward messages increase as we go to higher levels in the hierarchy only if ϵ is smaller than some threshold value. For ϵ larger than this threshold, instead, the messages become smaller, and it is not possible to reconstruct the highest levels in the hierarchy better than random chance.

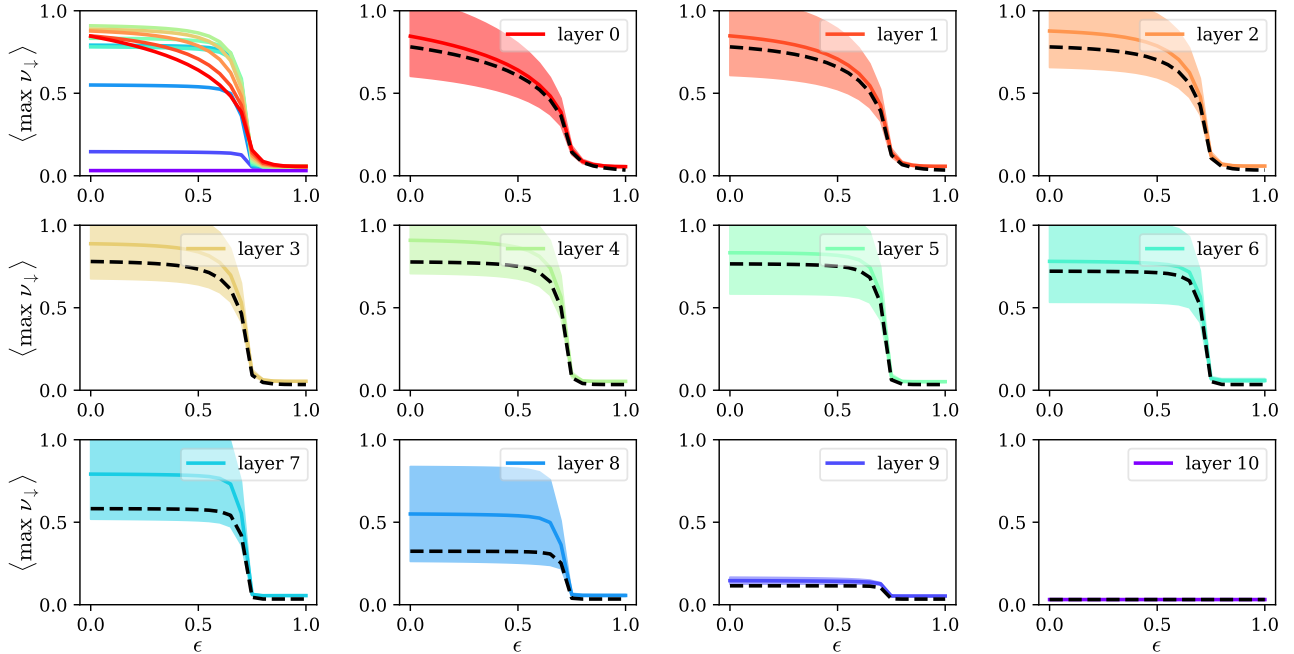


Figure 13. **Largest downward BP messages, averaged for each layer, for varying ϵ .** Data for the Random Hierarchical Model with the same parameters as Fig. 12. Each layer, indicated in the legend, is represented with a different colour, while the theoretical prediction from Eq. 54 is represented with the black dashed line. We observe that the messages in the downward process have large fluctuations, as represented by their standard deviations, especially for small ϵ . Still, the theory correctly captures the trend and becomes more accurate for increasing ϵ . The top left panel represents all the layers together for comparison. Starting from the initialization $\nu_{\downarrow} = 1/v$ at the top layer (10), we observe that the largest downward messages increase as we go to lower levels in the hierarchy only if ϵ is smaller than some threshold value.

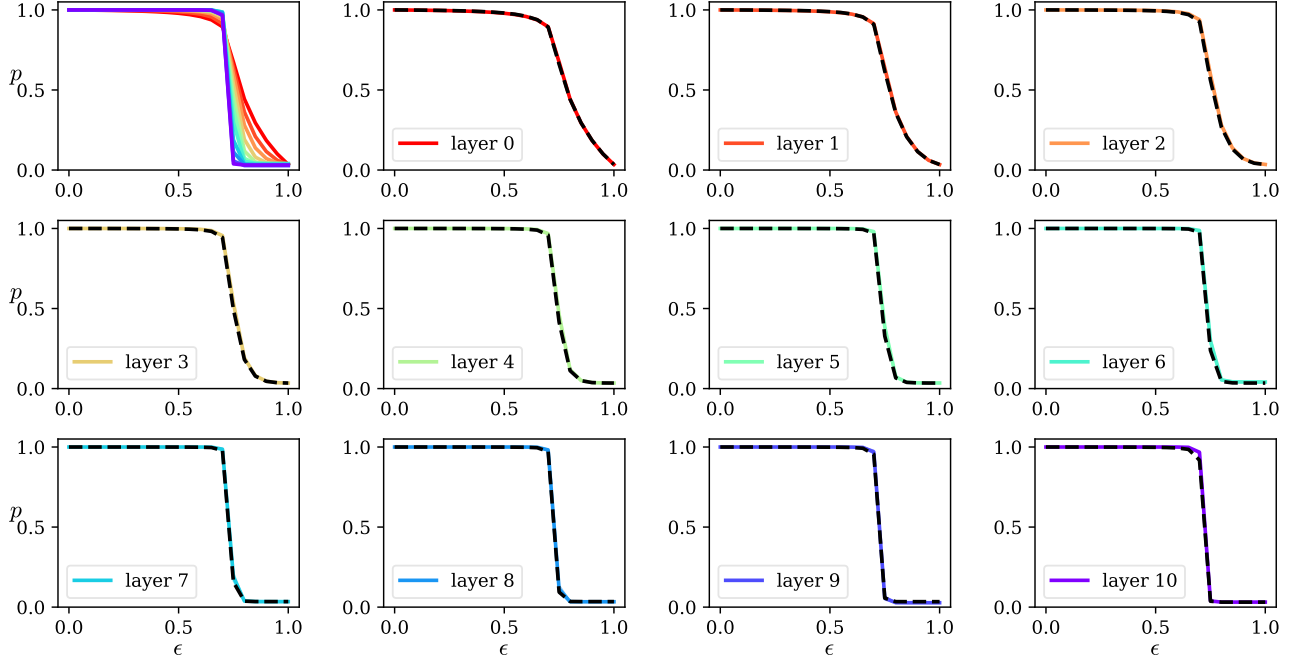


Figure 14. Largest marginal probabilities computed by BP, averaged for each layer, for varying ϵ . Data for the Random Hierarchical Model with the same parameters as Fig. 12. Each layer, indicated in the legend, is represented with a different colour and the black dashed line is the theoretical prediction from Eq. 59, which shows excellent agreement with the experiments. The top left panel represents all the layers together for comparison, where the inversion between the top and bottom layers can be observed (same curves as Fig. 7 in the main text).

C. Mapping from time diffusion to ϵ noise

In the diffusion process for the Random Hierarchy Model defined in Section 4, the beliefs $\nu_{\uparrow}^{(0)}$ at the input variables vary stochastically in time, according to Equation (4). Instead, in the simplified model of noise considered in Section 5, at a given noise level ϵ , these beliefs are fixed to two possible values (cf. Equation (7)). To study whether the ϵ -process is an effective approximation of the time diffusion process, we define an effective $\epsilon(t)$ depending on the reverse time of diffusion. At each input node $X_i^{(0)}$, we consider the upward messages $\nu_{\uparrow}^{(0)}(x)$ associated to the values x that are different from the value of $X_i^{(0)}$ at time $t = 0$. Denoting them as ν_t , we define

$$\frac{\epsilon(t)}{v} = \langle \nu_t \rangle, \quad (60)$$

where the average $\langle \nu_t \rangle$ is performed over all the leaves variables i and the realizations of the dynamics. $\epsilon(t)$ increases exponentially in time, according to the noise schedule used in the diffusion process, as shown in the left panel of Figure 15. The probability of the correct reconstruction of a given node in the diffusion process is reported as a function of $\epsilon(t)$ in the right panel of Figure 15. We observe that the curves for different layers have similar behaviour to those of the ϵ -process presented in Figure 7 of the main text, confirming that the latter is an effective approximation of denoising diffusion.

D. Hidden activations for different architectures

We perform the experiments described in Section 2.3 using the internal representations of different deep convolutional architectures trained for image classification on ImageNet-1k. We consider the ResNet architecture (He et al., 2016) with varying width and depth: a ResNet 50 achieving 95.4% top-5 accuracy, a Wide ResNet 50 having 95.8% top-5 accuracy, and a ResNet 152 having 96.0% top-5 accuracy (TorchVision maintainers and contributors, 2016). The results of the experiments performed with the hidden representations of these architectures are reported in Figure 16 and show the same qualitative behaviour as the one observed for the ConvNeXt architecture in Figure 2: the cosine similarity exhibits a sharp transition for the logits, while it decays smoothly for the hidden representations at early layers.

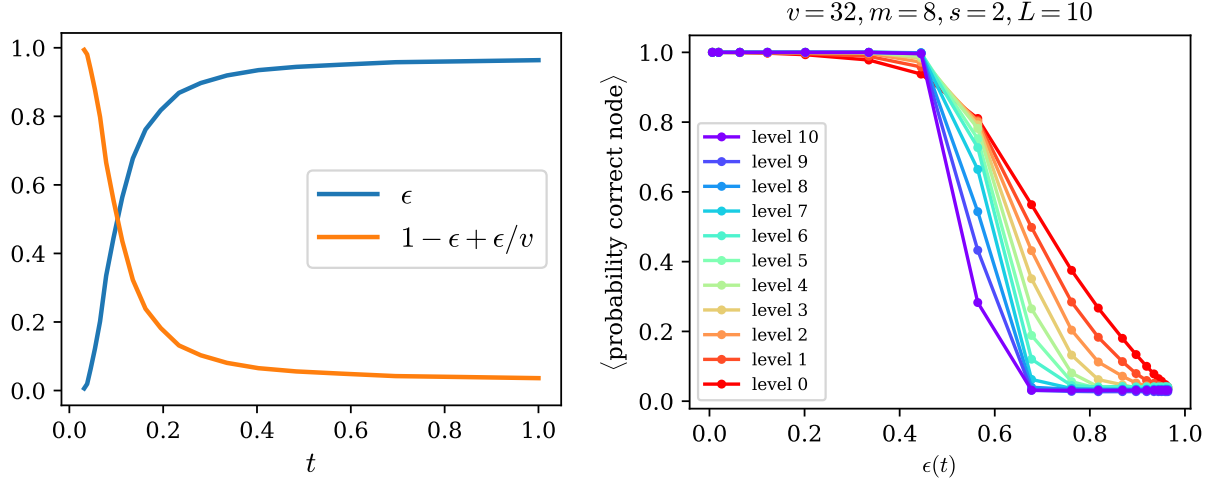


Figure 15. (Left panel) **Mapping between the ϵ values and the diffusion process.** From the average values of the beliefs at the leaves variables during the diffusion process at time t , we compute an effective $\epsilon(t)$ as $\epsilon(t)/v = \langle \nu_{\uparrow}^{(0)}(x) \rangle$, for the values x different from the starting one, averaging over the realizations of the diffusion process. (Right panel) **Probability of reconstructing the initial values for the nodes at a given layer during the diffusion process in time, using the effective ϵ computed in the left panel.** We observe that the shape of the curves with respect to the effective noise $\epsilon(t)$ is qualitatively similar to that of the simplified ϵ -process reported in Fig. 7, supporting that it represents a good approximation for studying the diffusion process in time.

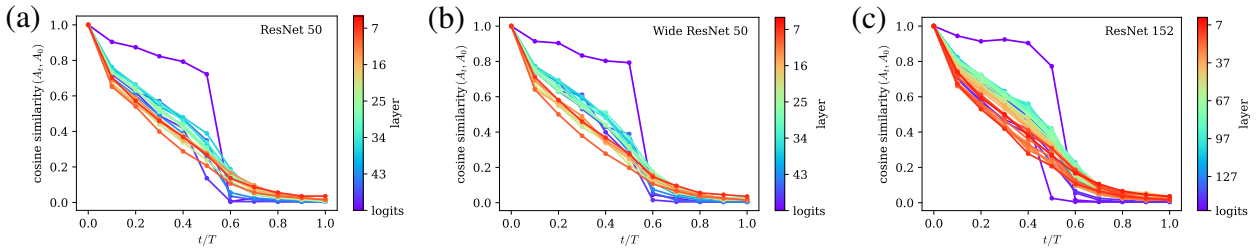


Figure 16. **Cosine similarity between the post-activations of the convolutional blocks of different ResNet architectures for the initial images x_0 and the synthesized ones $\hat{x}_0(t)$.** Specifically, panels (a), (b), and (c) correspond to ResNet50, Wide ResNet50, and ResNet152, respectively (He et al., 2016). As in Figure 2 for the ConvNeXt architecture, the similarity between logits exhibits a sharp drop around $t \approx T/2$, indicating the change in class, while the hidden representations of the early layers change more smoothly. To compute the cosine similarity, all activations are standardised, i.e., centred around the mean and scaled by the standard deviation computed on the 50000 images of the ImageNet-1k validation set. At each time, the cosine similarity values correspond to the maximum of their empirical distribution over 10000 images (10 per class of ImageNet-1k).